Model Flows for Chemical Vapor Deposition: Enforced Axial Flow and Temperature Dependent Viscosity.

Robert Miller[1]*, Paul T. Griffiths[2], Stephen J. Garrett[1]

ISROMAC 2017

International Symposium on Transport Phenomena and Dynamics of Rotating Machinery

Maui, Hawaii

December 16-21, 2017

Abstract

We present a numerical study concerning the enforced axial flow of a fluid with temperature dependent viscosity over a rotating disk. It is found that temperature dependencies in the liquid viscosity range narrow the mean velocity profiles and expand the mean temperature profile, while gaseous viscosity behaviour has the reverse effect in both of these cases. Under moderate axial flow the radial, azimuthal and temperature profiles are all entrained closer to the disk surface and the effects of variable viscosity are diminished. A linear stability analysis is performed over an extended range of axial flow strengths and temperature dependencies. Increasing the viscosity temperature-dependence parameter results in both Type I and II modes initially stabilising, before reaching a turning point and destabilising again. Enforced axial flow results in a stabilising effect of the Type I mode for all viscosity temperature-dependencies measured. Weakly enforced axial flow initially destabilises the Type II mode, before restabilising with further increased axial flow strength. The application of the investigated effects are discussed in the context of a chemical vapor deposition reactor.

Keywords

Boundary Layer Stability — Rotating Disk — Chemical Vapor Deposition

[1] *Department of Engineering, University of Leicester, Leicester, United Kingdom*

[2] *Department of Mechanical Engineering and Mathematical Sciences, Oxford Brookes University, Oxford, United Kingdom*

*__Corresponding author__: rm469@le.ac.uk

INTRODUCTION

Since the pioneering study of Von Kármán [1], the flow over a rotating disk of infinite radius has arguably become one of the most well studied systems in fluid mechanics. Early interest in the rotating disk was largely due to the inflectional velocity profile and presence of crossflow vortices that also appear in the flow over a swept wing, allowing for research into the latter medium through the more favourable geometry of the disk. This interest was further developed by Gregory et al. [2], through their clay disk visualisations of crossflow vortices attributed to linear disturbances. However, in recent years, modelling of industrial processes that utilise a rotating disk has become more commonplace, such as electrochemical cells [3, 4], hard disk drives [5], spin coating [6], and – of particular interest here – chemical vapour deposition (CVD) [7].

While the rotating disk model is typically considered an isothermal system, in many industrial applications the temperature of the disk and its surroundings cannot be neglected. As such, it is important to acknowledge the presence of temperature gradients. Gregg & Sparrow [8] investigated the heat transfer to a fluid from a heated rotating disk, but with the assumption of constant physical properties of the fluid. It is well established that properties such as transport coefficients, density, and viscosity are all sensitive to temperature changes. The variation of viscosity with temperature is investigated by Ling & Dybbs [9] through the forced flow over a flat plate, using an inverse linear relationship between viscosity and temperature. Kafoussias & Williams [10] examine free–forced convective flow with temperature dependent viscosity over a heated flat plate, finding that a reduction in the mean temperature flow profile through a more sensitive temperature–viscosity relationship results in a reduction of the boundary layer thickness. Hossain et al. [11] apply the same inverse linear relationship as Ling & Dybbs [9] to an MHD flow over a heated rotating disk, finding that the boundary layer narrows independently of a magnetic field. Regarding linear stability, Wall & Wilson [12] study temperature dependent viscosity in a channel flow, discovering that increasing viscosity due to the change in temperature across the channel results in a stabilisation of the flow. Most recently, Jasmine & Gajjar [13] model the boundary layer stability of a stationary fluid with temperature dependent viscosity over a heated rotating disk; they found that the neutral curves and overall stability of the flow were highly sensitive to changes in the temperature–viscosity relationship.

There is a wealth of literature concerning flows over rotating media, most of which set the fluid as initially stationary, with the flow a result of the rotation of the neighbouring geometry. More recent studies (both experimental and theoretical) examine the effects of an oncoming flow over rotating media to better understand transitional flows in industrially relevant configurations. Chen & Mortazavi [14] produced a model of a CVD reactor featuring a forced flow parameter to represent the injection of the gas into the system. Garrett et al. [15] present a linear stability analysis (both asymptotic and numerical) of the enforced axial flow over a rotating cone, where it is found that a stronger axial flow results in

delaying the onset of transition in both types of instability. This is extended to a more detailed study of the flow over a rotating disk [16], where a similar result is found.

Of particular interest is CVD: a microfabrication process used to produce thin epitaxial films and "two–dimensional" materials such as graphene. CVD is a method favoured for its ability to produce large area films of high–consistency thickness [17]. The product quality is reliant on a laminar gas flow, with quoted reactor Reynolds numbers of ∼100 in a rotating pedestal CVD reactor [18]. However, linear stability analyses of the flow over a rotating disk of infinite radius suggest that transitional flows are attained at Reynolds numbers as low as ∼200 [19]. When considering the influence of the CVD reactor conditions on the properties of the gas, it is possible that the onset of instability could appear at Reynolds numbers well within the operating range quoted. Furthermore, an increasing demand for the production of larger area films creates necessity for the examination of the limits of stability of the gas flow in a CVD reactor. Due to the high temperature gradients present in CVD, along with the gas injection perpendicular to the growth site (in a rotating pedestal reactor, specifically), temperature dependent viscosity and enforced axial flow are both parameters that are appropriate to include in a model of the flow in a CVD reactor. To the author's best knowledge, while others have produced models of CVD reactors [14, 18, 20, 21, 22, 23, 24], no comprehensive model flow yet exists, particularly with linear stability considered.

In this study, the effects of enforced axial flow and temperature dependent viscosity on an incompressible, Newtonian flow over a heated rotating disk of infinite radius are investigated. The study begins with a mathematical formulation of the mean flow from the Navier–Stokes equations. The method of the linear stability analysis is then outlined and the system of perturbation PDEs formulated. The results section addresses the effects of varying the axial flow and temperature dependence parameters; firstly on the mean flow behaviour and secondly on the neutral curves. Finally, we discuss the involvement of these factors in the future development of a sophisticated CVD–reactor flow model.

1. METHODS

We begin by considering a heated disk of infinite radius, rotating at angular velocity Ω^* about the z^* axis, with radial and azimuthal coordinates of r^* and θ, respectively (see Figure 1). An asterisk superscript indicates a dimensional quantity. The disk is situated downstream from an enforced flow incident parallel to the z^* axis. The fluid moves with radial, azimuthal and axial velocities of u^*, v^* and w^*, respectively.

At the edge of the boundary layer, the free stream velocity is described by the potential flow solution, $U_F^* = C^* r^*$, where C^* is a scaling factor determined by the free stream axial flow incident on the disk surface. The potential flow solution is related to the radial pressure component as

$$U_F^* \frac{\partial U_F^*}{\partial r^*} = -\frac{1}{\rho^*} \frac{\partial p^*}{\partial r^*},$$

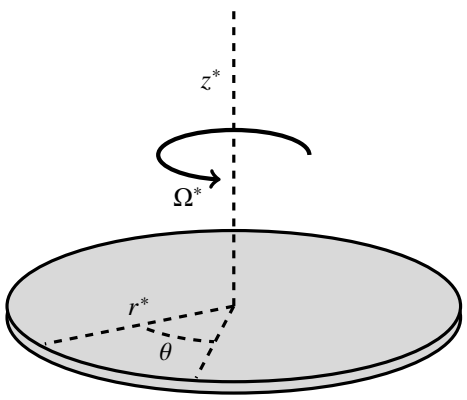

Figure 1. Coordinate system.

where ρ^* is the density of the fluid, and p^* is the pressure.

The temperature of the disk is fixed and results in a temperature gradient through the boundary layer. It is then assumed that the viscosity, μ^*, is dependent on the temperature, T^*, via

$$\mu^* = \frac{\mu_\infty^*}{1 + \gamma^*(T^* - T_\infty^*)},$$

where μ_∞^* and T_∞^* are the viscosity and temperature of the fluid at upstream infinity (i.e. at the point of injection), respectively. Here, γ^* is the control parameter in inverse temperature units. It is noted that γ^* is a characteristic of the fluid, and cannot be adjusted in an experimental context without fundamentally changing the fluid.

The modified Navier–Stokes equations in the rotating frame are then

$$\nabla^* \cdot \mathbf{U}^* = 0, \tag{1}$$

$$\rho^* \left(\frac{d\mathbf{U}^*}{dt^*} + \Omega^* \wedge \Omega^* \wedge \mathbf{r}^* \right) + 2\Omega^* \wedge \mathbf{r}^* = -\nabla^* p^* + (\nabla^* \cdot \mu^* \nabla^*)\mathbf{U}^*, \tag{2}$$

$$\rho^* C_p^* \frac{dT^*}{dt^*} = k^* \nabla^{*2} T^*, \tag{3}$$

where $\mathbf{U}^* = (u^*, v^*, w^*)$, C_p^* is the specific heat of the fluid, and k^* is the diffusion constant.

1.1 Mean Flow

The mean flow relative to the disk is a variation on the familiar Von Kármán solutions [1]. The dimensionless mean flow variables are functions of z^* and are given as

$$U(z) = \frac{u^*}{r^*\Omega^*},\ V(z) = \frac{v^*}{r^*\Omega^*},\ W(z) = \frac{w^*}{\sqrt{\nu^*\Omega^*}},$$

$$P(z) = \frac{p^*}{\rho^*\nu^*\Omega^*},\ \Theta(z) = \frac{T^* - T_\infty^*}{T_w^* - T_\infty^*},$$

where $z = z/L^*$ is the non–dimensionalised axial coordinate, $L^* = \sqrt{\nu^*/\Omega^*}$ is the length scale associated with the boundary layer thickness and $\nu^* = \mu^*/\rho^*$. Substituting these into equations 1 through 3 reduces the flow exactly to the following set of ordinary differential equations.

$$2U + W' = 0, \tag{4}$$

$$\varepsilon\Theta' U' + (1+\varepsilon\Theta)^2[U^2 - (V+1)^2 + U'W - T_S^2] - (1+\varepsilon\Theta)U'' = 0, \tag{5}$$

$$\varepsilon\Theta' V' + (1+\varepsilon\Theta)^2[2U(V+1) + V'W] - (1+\varepsilon\Theta)V'' = 0, \tag{6}$$

$$\varepsilon\Theta' W'(1+\varepsilon\Theta)^2(WW' + P') - (1+\varepsilon\Theta)W'' = 0, \tag{7}$$

$$\mathrm{Pr}\Theta' W - \Theta'' = 0; \tag{8}$$

where Pr is the Prandtl number. Equations 4 through 8 are subject to the boundary conditions

$$U(0) = V(0) = W(0) = \Theta(0) - 1 = 0,$$

$$U(z \to \infty) - T_S = V(z \to \infty) + 1 = \Theta(z \to \infty) = 0.$$

The boundary conditions represent no–slip on the disk surface and continuity with the outer flow at the upper edge of the boundary layer. Here, $T_S = C^*/\Omega^*$ is the axial flow strength parameter, the derivation of which can be seen in Garrett et al. [15] in the case of axial flow incident on a cone. The derivation for axial flow over a disk is the same as that of the cone with the half angle applied as 90°. Through non–dimensionalising, the temperature control parameter is replaced by the constant $\varepsilon = \gamma^* \cdot (T_w^* - T_\infty^*)$. Under the assumption that the disk temperature is greater than that of the fluid, $\varepsilon > 0$ represents the behaviour of a liquid viscosity under variable temperature, while $-1 < \varepsilon < 0$ represents the viscous behaviour of a gas. The interpretation of ε is reversed if $T_\infty^* > T_w^*$ i.e. the disk is cooled, rather than heated.

Equations 4 through 8 are solved via a 4th order Runge–Kutta iterative method employed alongside a two–dimensional Newton–Raphson searching routine. Upstream infinity is treated as $z = 20$, as this is found to be sufficient for the numerical solutions to reach convergence .

1.2 Stability Analysis

The velocity and pressure variables are now each subject to a small perturbation, while the temperature variable is deliberately left unperturbed. In Jasmine & Gajjar [13], the neutral curves prove to be incredibly sensitive to very small changes in ε (an increase from $\varepsilon = 0$ to 0.01 results in decreases of ~30 and ~100 of the upper and lower branch critical Reynolds numbers, respectively). It is possible that the introduction of temperature perturbations introduces a new mode of instability, such as in Mangiavacchi et al. [4] where a concentration dependent viscosity results in what they describe as "chemical modes" in the neutral curves. It can be seen in Jasmine & Gajjar [13] that the stability curves differ greatly from the usual two lobe structure encountered in much of the literature concerning boundary layer stability of rotating disks. As such, to avoid the introduction of "thermal modes", the temperature variables have been left unperturbed in order to only study the hydrodynamic stability of the flow.

Equations 1 through 3 are non–dimensionalised by the perturbing velocity, time and pressure scales as $(u, v, w) = (u^*, v^*, w^*)/r_s^*\Omega^*$, $t = t^* r_s^* \Omega^*/L^*$ and $p = p^*/\rho^* r_s^{*2}\Omega^{*2}$, respectively. The perturbed velocity and pressure variables are

$$u = \frac{r}{Re}U(z) + \hat{u}(r,\theta,z,t),\ v = \frac{r}{Re}V(z) + \hat{v}(r,\theta,z,t),$$

$$w = \frac{1}{Re}W(z) + \hat{w}(r,\theta,z,t),\ p = \frac{1}{Re^2}P(z) + \hat{p}(r,\theta,z,t),$$

which are then substituted into the non–dimensionalised Navier–Stokes equations. Here, $Re = r_s^*\Omega^* L^*/\nu^* = r_s^*/L^* = r_s$ is the local Reynolds number, fixed at radial position r_s^*. The resulting stability equations are then subject to a parallel flow approximation, wherein r coefficients are replaced by Re to reflect the constant thickness of the boundary layer across the disk. As such, for a fixed spin rate, r_s is interpreted as the non–dimensional radial position from the axis of rotation. Following this, the stability equations become fully separable, and so are expressed in modal form

$$[\hat{u}, \hat{v}, \hat{w}, \hat{p}] = [\tilde{u}(z), \tilde{v}(z), \tilde{w}(z), \tilde{p}(z)] \exp[i(\alpha r + \beta\theta - \omega t)].$$

Here, $\alpha = \alpha_r + i\alpha_i$ is the radial wave number, β is interpreted as the integer number of vortices around the azimuth, and ω is the disturbance frequency. In this study, we investigate vortices that are stationary relative to the disk, for which $\omega = 0$, though it is important that non-zero disturbance frequencies be considered in future (see §3.1).

The stability equations are linearised with respect to perturbation quantities and solved via a Galerkin projection method using Chebyshev polynomial decomposition. The use of transformation variables to form and solve a set of perturbation ODEs is a familiar method in a great deal of boundary layer stability literature. However, the method used here and presented by Appelquist & Imayama [25] eliminates the need for transformation and provides higher accuracy solutions.

2. RESULTS AND DISCUSSION

2.1 Mean Flow

Figure 2 shows the base flow profiles for U, V, W, and Θ for a gaseous viscosity ($\varepsilon = -0.5$), a temperature independent viscosity ($\varepsilon = 0$), and a liquid viscosity ($\varepsilon = 0.5$). Figure

3 shows the same profiles under moderate enforced axial flow ($T_s = 0.15$). The profiles for $\varepsilon = 0$ match those seen in Hussain et al. [16]. Increasing ε appears to entrain the fluid closer to the disk in the radial and azimuthal profiles, with both displaying increasingly steep gradients beyond their respective peaks. This is described by Jasmine & Gajjar [13] as a thinning of the boundary layer, which appears to hold true at higher axial flow strengths in the radial and azimuthal flow profiles.

The effects of axial flow are most prominent in the radial and axial profiles. The change in the radial velocity is as expected; U converges on T_S at a certain distance from the disk. In the axial profile, rather than the rapid convergence to a constant velocity above the disk as in the case of $T_S = 0$, the outflow accelerates with increasing distance from the disk. It is important to note that this effect is not physical; the linear relation that the profile takes on implies that the fluid approaches the boundary layer with unbounded speed for $T_S > 0$, but this is instead a result of the boundary layer approximation (a similar effect is noted in Hussain et al. [16]). Enforced axial flow appears to have a narrowing effect on the azimuthal and temperature profiles. The effect on the temperature profile in particular suggests that enforced axial flow can dominate thermal effects, as there is little to no variation in the different ε curves for $T_s = 0.15$.

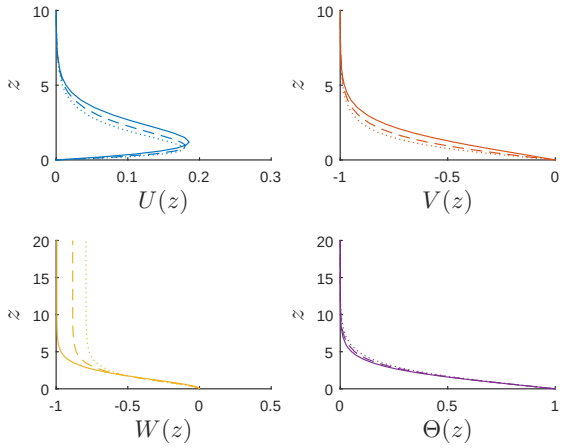

Figure 2. Mean flow plots for $T_s = 0$. Solid line: $\varepsilon = -0.5$. Dashed line: $\varepsilon = 0$. Dotted line: $\varepsilon = 0.5$.

2.2 Stability Analysis

Figures 4 to 6 show the resulting neutral curves for various values of ε and T_S, while Tables 1 to 3 display the physical attributes of each neutral curve. It should be noted that the number of vortices (β) have been rounded up to the nearest integer value for consistency with the physical interpretation. It appears initially that with respect to temperature dependence, the most stable curve is that of $\varepsilon = 0$; imposing temperature dependence values in the range of gaseous or liquid behaviour results in a reduced critical Reynolds number. Conversely, it can be seen that increasing T_S appears to have

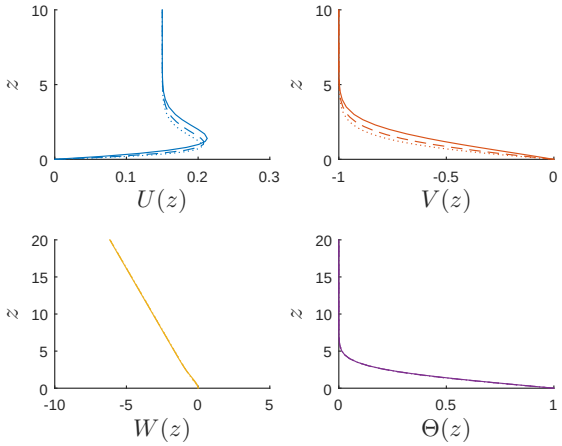

Figure 3. Mean flow plots for $T_s = 0.15$. Solid line: $\varepsilon = -0.5$. Dashed line: $\varepsilon = 0$. Dotted line: $\varepsilon = 0.5$.

a generally stabilising effect; pushing the critical Reynolds number to higher values. However, for the gaseous viscosity curves, higher strength axial flow appears to contribute to a destabilising of the Type II branch.

Figures 7 & 8 display a more nuanced relation between the control parameters and the Type I and Type II critical Reynolds numbers, respectively. From Figure 7 it can be seen that as ε is increased, shifting from gaseous behaviour to liquid, the Type I critical Reynolds number also increases and as such the flow becomes more stable. However, this trend continues into the small positive values of ε, before reaching a turning point beyond which a higher sensitivity decreases the critical Reynolds number. This suggests that there is a small range of liquid viscosity sensitivities that result in a more stable flow as opposed to a fluid without a temperature dependent viscosity. Figure 7 also suggests that increasing T_S has a stabilising effect on the type I mode for all of the ε values studied, and also results in shifting the turning point to a slightly higher value of ε. The type II mode appears to have a similar relationship with increasing T_s as the type I mode does with ε, in that $T_s = 0.05$ exhibits a lower type II critical Reynolds number than $T_s = 0$, which then increases with all subsequent values of T_s. This relationship is more evident in Figure 8, where the majority of the $T_s = 0.05$ curve sits below that of the $T_s = 0$ curve. It is likely that with smaller increments of T_s applied, there would be a visible turning point in the range $0 < T_s < 0.15$ where the type II mode begins to stabilise.

3. CONCLUSION

We have examined the mean flow and boundary layer stability data for the flow of an incompressible fluid with temperature dependent viscosity over a heated rotating disk.

In the mean flow analysis, it is seen that increasing ε results in a narrowing of the boundary layer, where the main activity in the velocity profiles occurs closer to the disk sur-

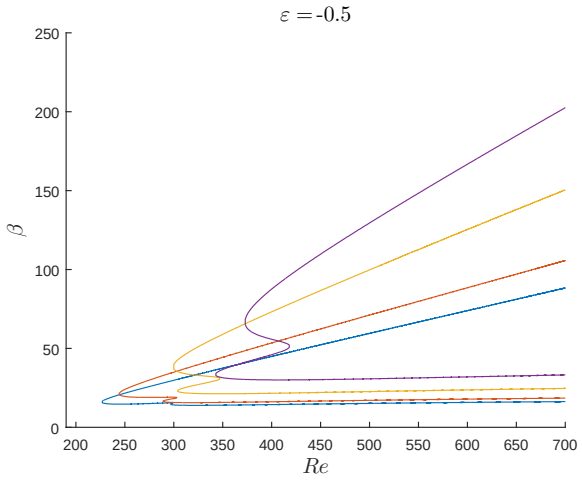

Figure 4. Neutral curve plots for $\varepsilon = -0.5$. From left to right, $T_S = 0, 0.05, 0.15, 0.25$.

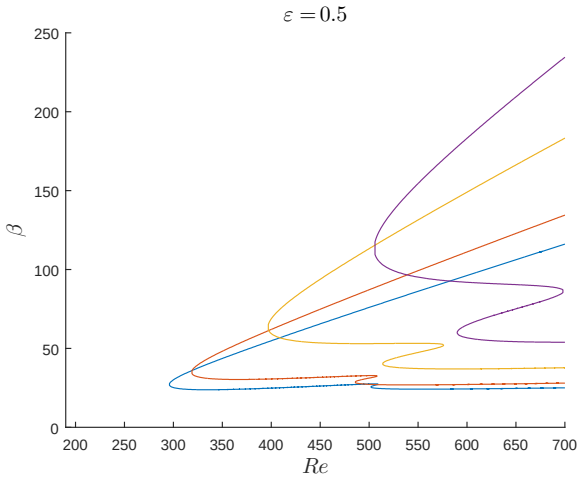

Figure 6. Neutral curve plots for $\varepsilon = 0.5$. From left to right, $T_S = 0, 0.05, 0.15, 0.25$.

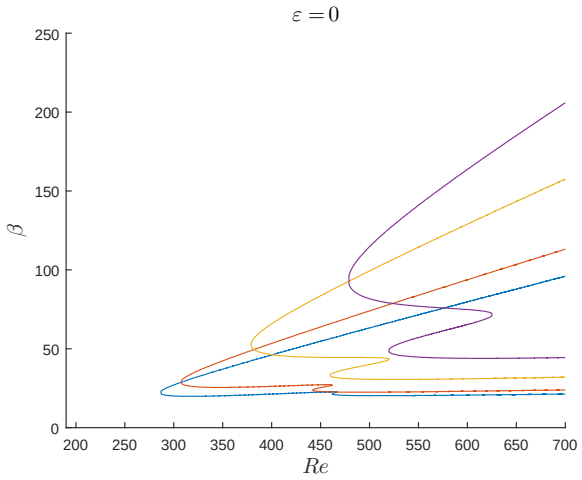

Figure 5. Neutral curve plots for $\varepsilon = 0$. From left to right, $T_S = 0, 0.05, 0.15, 0.25$.

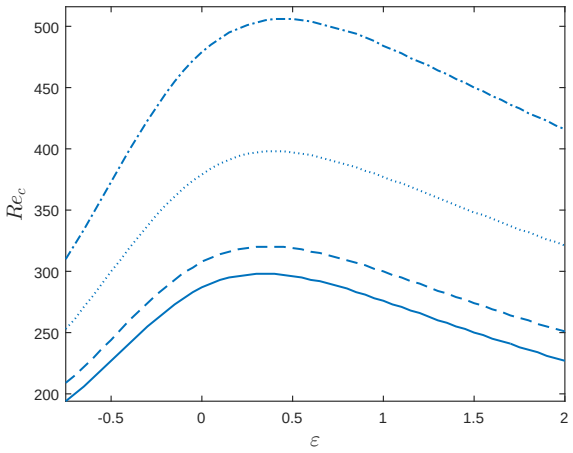

Figure 7. Type I critical Reynolds number for different ε values. Solid line: $T_s = 0$. Dashed line: $T_s = 0.05$. Dotted line: $T_s = 0.15$. Dot-dashed line: $T_s = 0.25$.

face, while broadening the mean temperature profile. Applying $T_s = 0.15$ suppresses the effect of varying ε in the mean flow profiles – most significantly in the axial profile.

In the stability analysis, the neutral curves suggest that any non–zero value of ε results in a lower critical Reynolds number and a destabilising effect on both branches, while increasing T_s results in an overall stabilising effect. Upon plotting the critical Reynolds numbers against the corresponding ε value, it is seen that there is, in fact, a small range of positive ε values that are more stable than a temperature independent viscosity, beyond which the fluid begins to more drastically destabilise.

This study considered only stationary modes of instability. It is often the case that travelling modes are more unstable than their stationary counterparts [13, 16, 26]. Jasmine & Gajjar [13] noted that the destabilising effect of increasing ε was consistent between both stationary and travelling modes, and extended to the onset of absolute instability. Hussain et al. [16] also noted that the stabilising effect of enforced axial flow was consistent between stationary and travelling modes. As such, it is likely that the effects of competing parameters ε and T_s would likely produce the same effects as seen for stationary modes (though it is acknowledged that the formulated stability equations in this study are different to those in Jasmine & Gajjar [13], both through different results of derivation and through their use of multiple scale variables as opposed to our parallel flow approximation). The natural progression from studying travelling modes would be to measure growth rates and absolute instability.

3.1 Relevance to CVD reactors

Our preliminary results can be interpreted in the context of CVD reactors. In particular, recall that we seek to extend the radial distance over which the flow remains laminar. We see from Figure 7 that the extent of the inviscidly stable regime

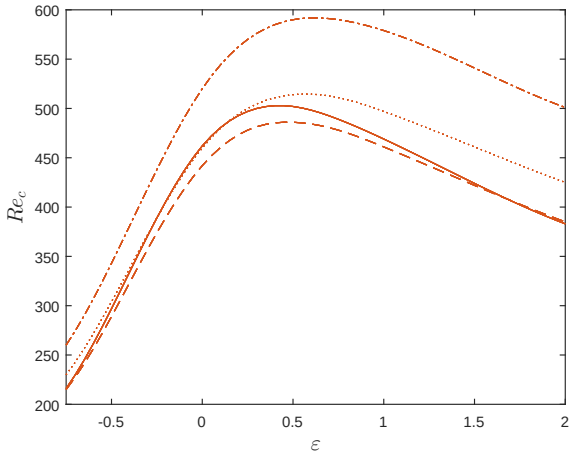

Figure 8. Type II critical Reynolds number for different ε values. Solid line: $T_s = 0$. Dashed line: $T_s = 0.05$. Dotted line: $T_s = 0.15$. Dot-dashed line: $T_s = 0.25$.

Table 1. Values of critical Reynolds number for both branches of instability (Re_c), number of vortices (β) and wave angle (ϵ) for various values of axial flow strength (T_s) where $\varepsilon = -0.5$. Bracketed headings indicate Type II values.

$\varepsilon = -0.5$						
T_s	Re_c	β	ϵ	(Re_c)	(β)	(ϵ)
0	227	17	11.2	297	15	18.8
0.05	244	22	12.5	289	17	19.9
0.15	300	40	16.3	304	24	27.7
0.25	373	69	20.3	343	35	25.9

can be optimised using a delivery gas with temperature sensitivity between $-0.2 < \varepsilon < 0.6$ (although it is acknowledged that positive values of ε are usually characteristic of fluids, rather than gases). This would place the operation of the reactor around the maxima of the curves in Figurs 7 where the extent of the laminar flow is most receptive to the incident axial flow rate. The extent of the stable region could then be controlled by increasing the axial flow rate. The limit of this beneficial behaviour beyond $T_s = 0.25$ is, however, currently unknown from our preliminary model.

While we have shown here that enforced axial flow and temperature dependent viscosity are both crucial factors for any model of a rotating disk CVD reactor, these alone are not sufficient for a complete model. In particular, temperature dependencies should extend to all physical properties of the fluid according to Kleijn [7]. This would suggest that a compressible model would also be necessary, which has been acknowledged in other approaches [20, 21, 18]. Conversely, Jensen et al. [22] states that the inlet Mach number is typically low enough for compressibility effects to be neglected. With this in mind, it is likely that future work will continue to utilise an incompressible approach, though it is recognised that a more sophisticated model will require the measurement of compressibility effects.

Table 2. Values of critical Reynolds number for both branches of instability (Re_c), number of vortices (β) and wave angle (ϵ) for various values of axial flow strength (T_s) where $\varepsilon = 0$. Bracketed headings indicate Type II values.

$\varepsilon = 0$						
T_s	Re_c	β	ϵ	(Re_c)	(β)	(ϵ)
0	287	24	11.5	462	22	19.5
0.05	308	31	12.8	442	24	20.2
0.15	379	53	16.2	460	34	22.7
0.25	479	97	20.2	520	50	25.7

Table 3. Values of critical Reynolds number for both branches of instability (Re_c), number of vortices (β) and wave angle (ϵ) for various values of axial flow strength (T_s) where $\varepsilon = 0.5$. Bracketed headings indicate Type II values.

$\varepsilon = 0.5$						
T_s	Re_c	β	ϵ	(Re_c)	(β)	(ϵ)
0	296	28	11.8	502	26	19.7
0.05	319	36	13.0	486	29	20.5
0.15	397	66	16.3	514	41	22.6
0.25	506	118	20.3	590	61	25.5

For a further developed model of CVD, it is imperative that both stationary and travelling modes of instability are investigated. In the growth of graphene via CVD, in situ roughness is largely influenced by the growth substrate. For example, for graphene grown on copper, the growth sites appear as multiple islands which eventually join to form a cohesive film. This could manifest as surface roughness that would influence the presence of stationary vortices. Conversely, graphene growth on nickel involves absorption of carbon atoms into the substrate bulk, the film then produced via adsorption through cooling. As such, the nickel substrate would likely be consistently smooth throughout the process, suggesting that travelling instabilities may take precedent. The difference between using a polycrystalline or monocrystalline substrate also produces the same surface roughness argument, as a polycrystalline substrate has grain boundaries that could constitute surface roughness.

Perhaps the main motivation for any CVD model is to measure what mechanisms affect the film growth. The primary focus of Chen & Mortazavi [14] was the effects on the growth rate with varying physical parameters (e.g. Prandtl number). It would be simple to include a concentration/species continuity equation, but from a stability perspective it would be necessary to couple this equation to the other constituent equations. Mangiavacchi et al. [4] achieve this in their model of an electrochemical cell through a concentration dependent viscosity. The incorporation of both temperature and concentration dependence on the viscosity is the next stage

in this ongoing project.

ACKNOWLEDGMENTS

R Miller would like to thank the Engineering and Physical Sciences Research Council for providing the funding for this research.

REFERENCES

[1] T. von Kármán. Über laminare und turbulente reibung. *ZAMM - Journal of Applied Mathematics and Mechanics / Zeitschrift für Angewandte Mathematik und Mechanik*, 1(4):233–252, 1921.

[2] N Gregory, JT Stuart, and WS Walker. On the stability of three-dimensional boundary layers with application to the flow due to a rotating disk. *Philosophical Transactions of the Royal Society of London A: Mathematical, Physical and Engineering Sciences*, 248(943):155–199, 1955.

[3] J. Pontes, N. Mangiavacchi, A. R. Conceição, O. E. Barcia, O. R. Mattos, and B. Tribollet. Rotating disk flow stability in electrochemical cells: Effect of viscosity stratification. *Physics of Fluids*, 16(3):707–716, 2004.

[4] N Mangiavacchi, J Pontes, OE Barcia, OR Mattos, and B Tribollet. Rotating disk flow stability in electrochemical cells: Effect of the transport of a chemical species. *Physics of Fluids (1994-present)*, 19(11):114109, 2007.

[5] Majid Molki and Manoj Kumar Nagalla. Flow characteristics of rotating disks simulating a computer hard drive. *Numerical Heat Transfer, Part A: Applications*, 48(8):745–761, 2005.

[6] Masahiro Yanagisawa. Slip effect for thin liquid film on a rotating disk. *Journal of applied physics*, 61(3):1034–1037, 1987.

[7] C. R. Kleijn. On the modelling of transport phenomena in chemical vapour deposition and its use in reactor design and process optimization. *Thin Solid Films*, 206(1–2):47–53, 1991.

[8] JL Gregg and EM Sparrow. Heat transfer from a rotating disk to fluids of any prandtl number. 1959.

[9] JX Ling and A Dybbs. Forced convection over a flat plate submersed in a porous medium: variable viscosity case. Report, American Society of Mechanical Engineers, New York, NY, 1987.

[10] NG Kafoussias and EW Williams. The effect of temperature-dependent viscosity on free-forced convective laminar boundary layer flow past a vertical isothermal flat plate. *Acta Mechanica*, 110(1):123–137, 1995.

[11] Md Anwar Hossain, Akter Hossain, and Mike Wilson. Unsteady flow of viscous incompressible fluid with temperature-dependent viscosity due to a rotating disc in presence of transverse magnetic field and heat transfer. *International journal of thermal sciences*, 40(1):11–20, 2001.

[12] DP Wall and SK Wilson. *The linear stability of channel flow of fluid with temperature-dependent viscosity*, pages 416–423. Springer, 1997.

[13] H. A. Jasmine and J. S. B. Gajjar. Absolute and convective instabilities in the incompressible boundary layer on a rotating disk with temperature-dependent viscosity. *International Journal of Heat and Mass Transfer*, 48(5):1022–1037, 2005.

[14] K. Chen and A. R. Mortazavi. An analytical study of the chemical vapor deposition (cvd) processes in a rotating pedestal reactor. *Journal of Crystal Growth*, 76(1):199–208, 1986.

[15] Stephen J Garrett, Zahir Hussain, and SO Stephen. Boundary-layer transition on broad cones rotating in an imposed axial flow. *AIAA Journal*, 48(6):1184–1194, 2010.

[16] Z. Hussain, S. J. Garrett, and S. O. Stephen. The instability of the boundary layer over a disk rotating in an enforced axial flow. *Physics of Fluids*, 23(11):114108, 2011.

[17] Sukang Bae, Hyeongkeun Kim, Youngbin Lee, Xiangfan Xu, Jae-Sung Park, Yi Zheng, Jayakumar Balakrishnan, Tian Lei, Hye Ri Kim, and Young Il Song. Roll-to-roll production of 30-inch graphene films for transparent electrodes. *Nature nanotechnology*, 5(8):574–578, 2010.

[18] S. P. Vanka, G. Luo, and N. G. Glumac. Parametric effects on thin film growth and uniformity in an atmospheric pressure impinging jet cvd reactor. *Journal of Crystal Growth*, 267(1–2):22–34, 2004.

[19] Helen L Reed and William S Saric. Stability of three-dimensional boundary layers. *Annual Review of Fluid Mechanics*, 21(1):235–284, 1989.

[20] Michael E Coltrin, Robert J Kee, and Greg H Evans. A mathematical model of the fluid mechanics and gas-phase chemistry in a rotating disk chemical vapor deposition reactor. *Journal of the Electrochemical Society*, 136(3):819–829, 1989.

[21] William G Breiland and Greg H Evans. Design and verification of nearly ideal flow and heat transfer in a rotating disk chemical vapor deposition reactor. *Journal of the Electrochemical Society*, 138(6):1806–1816, 1991.

[22] Klavs F. Jensen, Erik O. Einset, and Dimitrios I. Fotiadis. Flow phenomena in chemical vapor deposition of thin films. *Annual Review of Fluid Mechanics*, 23(1):197–232, 1991.

[23] RW Davis, EF Moore, and MR Zachariah. Numerical modeling of particle dynamics in a rotating disk chemical vapor deposition reactor. *Journal of crystal growth*, 132(3):513–522, 1993.

[24] Dean E Kassmann and Thomas A Badgwell. Modeling diamond chemical vapor deposition in a rotating disk reactor. *Diamond and related materials*, 5(3):221–225, 1996.

[25] Ellinor Appelquist and Shintaro Imayama. Revisiting the stability analysis of the flow over a rotating disk, 2014.

[26] R. J. Lingwood. Absolute instability of the boundary layer on a rotating disk. *Journal of Fluid Mechanics*, 299:17–33, 1995.